Anomalous resonance-enhanced harmonic ellipticity in an elliptically polarized laser field

Xiao-Xin Huo ©, Shuang Wang, Lin Sun, Yun-He Xing, Jun Zhang,* and Xue-Shen Liu†

Institute of Atomic and Molecular Physics, Jilin University, Changchun 130012, China

We investigate theoretically resonant harmonic generation in He^+ from an elliptically polarized laser field. The results show that there are two anomalous resonance-enhanced harmonics and the intensities of the anomalous resonance-enhanced harmonics remain unchanged for different laser ellipticities which are approximately two orders of magnitude stronger than those of nonresonant harmonics. We illustrate that the first resonance-enhanced harmonic is due to the transition between the ground state and the first excited state and the second one is due to the transition between the ground state and the second excited state. Our results also show that the enhancements of the harmonic intensities are related to the continuous collisions of the electron with the parent ion due to multiphoton resonance. The two resonance-enhanced harmonic intensities decrease gradually and orders do not change with an increase of the laser intensity, which can be illustrated through the Stark effect. The ellipticities of the two resonance-enhanced harmonics are approximately equal to the selected driving laser ellipticities regardless of the $\pm$ sign under different driving laser ellipticities, which might provide an accessible route toward characterizing the polarization properties of the laser. Our results offer a way for the generation of quasimonochromatic circularly polarized EUV radiation with high intensity.

I. INTRODUCTION

High-order harmonic generation (HHG) is a highly non-linear physical process by the interaction of laser radiation with different media, which can be successfully described by a three-step model [1]. High-order harmonic generation provides an ideal light source for the production of extreme ultraviolet (XUV), soft-x-ray, and attosecond pulses [2–4]. In recent years, the polarization properties of HHG have been widely investigated. In particular, for circularly polarized (CP) HHG with potential value in experiments, HHG can be used to show the circular dichroism of molecules [5,6], distinguish the enantiomerism of chiral molecules, and analyze the magnetic structure of materials [7,8].

Some sophisticated laser schemes have been proposed towards the generation of CP HHG. The bichromatic counter-rotating CP [9–11] and the orthogonally polarized two-color [12–14] laser fields have been recognized as effective means to generate CP or elliptically polarized (EP) HHG. However, due to the weak harmonic yield or low harmonic ellipticity, the application prospects of these schemes need further development. Recently, the EP laser field has been extensively adopted to investigate CP or EP HHG because the harmonic emission efficiency and ellipticity are sensitive to the driving laser ellipticity [15–20]. However, the harmonic ellipticity increases with the increase of the driving laser ellipticity, but the harmonic yield decreases exponentially with the increase of the driving laser ellipticity [21]. Thus, further effort is still needed to generate harmonics with high ellipticity and high intensity.

Generation of resonance-enhanced harmonics with high ellipticity is a considerable result. Resonance-enhanced HHG can increase the intensity of single harmonics by several orders of magnitude, which makes them excellent candidates for various applications [22,23]. The phase matching of the pump and harmonics by using gas-filled waveguides [24] and the interaction of the XUV radiation with the ablation medium [25], etc., are efficient ways to generate resonance-enhanced harmonics. The multiphoton resonance between the ground state and the Stark displacement excited state, the transition between the ground state and the excited state or the autoionizing state, and the electronic multiple recollisions processes have been demonstrated to be origins of enhancement of resonant harmonics [26–30].

Resonance-enhanced HHG with high ellipticity driven by the EP laser field has attracted extensive attention and may be a prospective candidate for a source of quasimonochromatic EP or even CP XUV radiation with relatively high intensity. The experiment performed by Ferré *et al*. [31] proposed that bright, coherent, and ultrashort quasicircular pulses can be generated in bichromatic counterrotating elliptically polarized laser fields by resonance-enhanced harmonics, which can be used to measure the photoelectron circular dichroism of chiral molecules. Recent investigations of elliptical properties through the interaction between the EP laser field and metal ions [32,33] have shown that resonance-enhanced harmonic generation is due to the transition between the ground state and an autoionizing state and the polarization of the single-order resonance-enhanced harmonic can be controlled by adjusting the driving laser ellipticity.

In this paper we investigate the ellipticity of the harmonics of He^+ in EP laser fields. Our results show that there are two resonance-enhanced harmonics for different driving laser ellipticities. The intensities of the resonance-enhanced

---

*junzhang@jlu.edu.cn
†liuxs@jlu.edu.cn

harmonics are two orders of magnitude stronger than those of nonresonant harmonics and do not change with the driving laser ellipticity. The first resonance-enhanced harmonic is generated due to the transition between the ground state and the first excited state; the second one is generated due to the transition between the ground state and the second excited state. Our result also demonstrates that the resonance enhancements of the harmonics originate from the continuous return of electrons to the parent ion. The two resonance-enhanced harmonic intensities decrease gradually and orders do not change with an increase of the laser intensity, which can be illustrated through the Stark effect. In addition, we find that the ellipticity of the nonresonant harmonics is irregular with an increase of the driving laser ellipticity, while that of the anomalous resonance-enhanced harmonics is approximately equal to the selected driving laser ellipticity without considering the ± sign. The results provide a way to characterize the polarization properties of the laser by the resonance-enhanced harmonic ellipticity. Our results achieve the quasimonochromatic EP or even CP EUV radiation with high and unchanged intensity.

II. THEORETICAL METHODS

We investigate the ellipticity of the harmonics when the target atom He^+ is exposed to an EP laser field by numerically solving the two-dimensional (2D) time-dependent Schrödinger equation (TDSE). The 2D TDSE in the dipole approximation and length gauge can be written as

$$i\frac{\partial \psi(x, y, t)}{\partial t} = \left[\frac{P_x^2 + P_y^2}{2} + V_C(x, y) \right.$$
$$\left. + xE_x(t) + yE_y(t) \right] \psi(x, y, t), \quad (1)$$

where $V_C(x, y)$ is the soft-core Coulomb potential between the electron and nucleus, which can be expressed as $V_C(x, y) = -2/\sqrt{x^2 + y^2 + a}$. The soft-core parameter $a = 0.169$ is used to eliminate the singularity of the potential function at the origin [34]. The ionization potential of the ground state evolved by the imaginary-time evolution method is $I_{p0} = 2$ a.u., which corresponds to the energy of the ground state of He^+. The energies of the first and second excited states that evolved are $I_{p1} = 0.65$ a.u. and $I_{p2} = 0.457$ a.u., respectively.

The driving laser field is elliptically polarized, which can be written as

$$E_x(t) = \frac{E_0}{\sqrt{1 + \varepsilon_D^2}} f(t) \cos(\omega_0 t),$$
$$E_y(t) = \frac{\varepsilon_D E_0}{\sqrt{1 + \varepsilon_D^2}} f(t) \sin(\omega_0 t), \quad (2)$$

where $f(t) = \sin^2(\frac{\pi t}{nT})$ is the envelope of the laser field with three optical cycles ($n = 3$), $\omega_0 = 0.065$ a.u. (700 nm) and $E_0 = 0.075$ a.u. (2×10^{14} W/cm^2) are the laser frequency and amplitude, respectively, ε_D is the driving laser ellipticity ranging from -1 to 1, and $\varepsilon_D > 0$ and $\varepsilon_D < 0$ represent the right-handed and left-handed polarized laser fields, respectively. The time-dependent dipole acceleration in the x and

y directions can be given by the Ehrenfest theorem

$$d_x(t) = \langle \psi(x, y, t)| - \frac{\partial V_C(x, y)}{\partial x} - E_x(t)|\psi(x, y, t)\rangle,$$
$$d_y(t) = \langle \psi(x, y, t)| - \frac{\partial V_C(x, y)}{\partial y} - E_y(t)|\psi(x, y, t)\rangle. \quad (3)$$

The corresponding HHG spectrum can be expressed by

$$F_x(\omega) = \left| \frac{1}{T - t_0} \int_{t_0}^{T} d_x(t) e^{-i\omega t} dt \right|^2,$$
$$F_y(\omega) = \left| \frac{1}{T - t_0} \int_{t_0}^{T} d_y(t) e^{-i\omega t} dt \right|^2. \quad (4)$$

The ellipticity of the high-order harmonics can be obtained by [35]

$$\varepsilon_H = \frac{(|a_+| - |a_-|)}{(|a_+| + |a_-|)}, \quad (5)$$

where

$$a_{\pm} = \frac{1}{\sqrt{2}}[a_x(\omega) \pm i a_y(\omega)], \quad (6)$$

with

$$a_{x,y}(\omega) = \int_{-\infty}^{\infty} d_{x,y}(t) e^{-i\omega t} dt \quad (7)$$

the x and y components of the dipole acceleration in the frequency domain, respectively. According to Eq. (5), the expression of the harmonic ellipticity can also be written [13,36]

$$\varepsilon_H = \pm \sqrt{\frac{1 + r^2 - \sqrt{1 + r^4 + 2r^2 \cos(2\delta)}}{1 + r^2 + \sqrt{1 + r^4 + 2r^2 \cos(2\delta)}}}, \quad (8)$$

where $r = |a_y(\omega)|/|a_x(\omega)|$ and $\delta = \phi_y(\omega) - \phi_x(\omega)$ is the phase difference of the x and y components of the harmonics, with $\phi_{x,y}(\omega) = \arg[a_{x,y}(\omega)]$. Here $\varepsilon_H > 0$ and $\varepsilon_H < 0$ represent the right-handed and left-handed harmonics, respectively.

III. RESULTS AND DISCUSSION

Figure 1(a) shows the harmonic spectrum of He^+ driven by the EP laser field with different driving laser ellipticities for a laser intensity of 2.0×10^{14} W/cm^2. We can see that there are two resonance-enhanced harmonic peaks for different driving laser ellipticities. The first and second peaks are located at H21 and H23 orders, respectively. The intensities of the resonance-enhanced (H21 and H23) harmonics are approximately two orders of magnitude stronger than those of the other nonresonant ones and are not affected by the driving laser ellipticity. We also find that the intensity of the nonresonant harmonics decreases rapidly with an increase of the driving laser ellipticity, which can be understood by the three-step model. In an EP laser field, the electron wave packet returning to the parent ion is transversely shifted relative to the parent ion, which leads to a decrease in the number of electrons returning to the parent ion. Thus, the harmonic intensity decreases rapidly with an increase of the driving laser ellipticity.
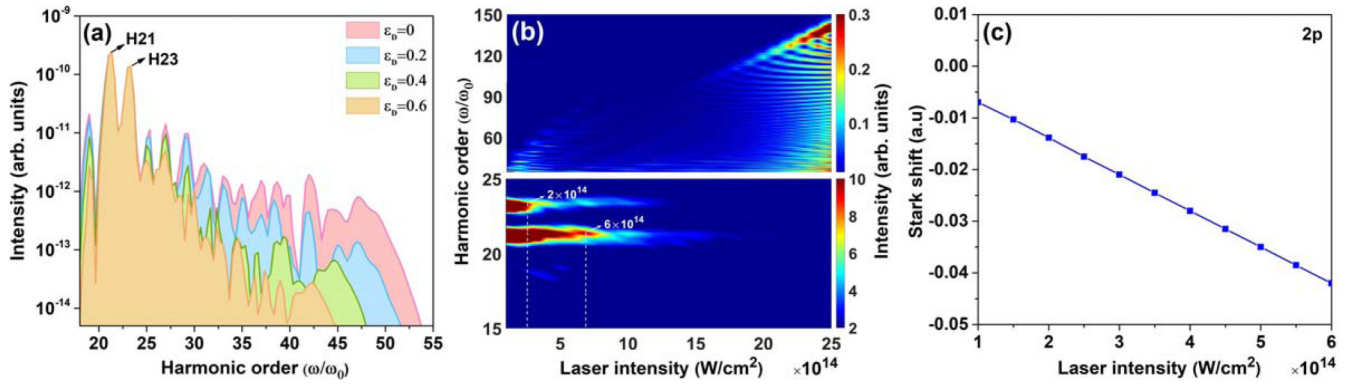
FIG. 1. (a) Harmonic spectrum with different driving laser ellipticities for the laser intensity 2.0×10^{14} W/cm^2. (b) Harmonic intensity distribution as a function of the laser intensity and the harmonic order with $\varepsilon_D = 0$. The colors indicate harmonic intensity. The upper panel and the lower panel indicate the intensities of the nonresonance and the resonance-enhanced harmonics with different laser intensity, respectively. (c) Stark shifts of the first excited state $2p$.

The resonant energy difference between the ground state and the first excited state $\Delta E_1 = I_{p0} - I_{p1} = 1.35$ a.u. $= 36.71$ eV, which is close to the energy of H21 (37.14 eV). The resonant energy difference between the ground state and the second excited state $\Delta E_2 = I_{p0} - I_{p2} = 1.543$ a.u. $= 41.98$ eV, which is close to the energy of H23 (40.68 eV). These indicate that the resonant peaks located at H21 and H23 are due to the bound-bound transitions, as illustrated in Ref. [37]. We have also demonstrated the time-dependent populations of the ground state and the excited states (the results are not shown here). We find that the time-dependent populations are transferred from the ground state to the first and second excited states due to the resonant excitation and transition processes, resulting in the resonance enhancements of H21 and H23.

The resonance enhancement of H21 and H23 cannot be illustrated by the three-step model. Instead, the four-step model should be considered to illustrate the mechanism of resonance enhancement. For the four-step model, the excitation is added prior to the three steps of HHG [38,39], i.e., the electron is first preexcited to the resonant bound state and tunnel ionized from the resonant excited state. Then the electron accelerates and recombines with the ground state to emit the HHG driven by the laser field. The part of the electron in the excited state will directly transit to the ground state, which leads to the resonance enhancement of the HHG. In this four-step model mechanism, the multiphoton resonance arises from the excitation and ionization steps [39]. The H21 and H23 are below-threshold harmonics, which are dominated by the multiphoton mechanism. Thus, the resonance enhancements of H21 and H23 are attributed to the excitation transition steps. In Ref. [38] Bian and Bandrauk demonstrated the strong resonance of the HHG from HeH^{2+} driven by the linearly polarized laser field. The results show that the strong resonance around H15 agrees with the energy difference between the ground state and the first excited state. In addition, the strong resonance cannot be illustrated by the three-step model, but rather by the four-step model described above. Our result agrees with the result illustrated in Ref. [38].

Figure 1(b) shows the harmonic intensity distribution as a function of the laser intensity (from 1.0×10^{14} to 2.5×10^{15} W/cm^2) and the harmonic order for a laser wavelength

of 700 nm with $\varepsilon_D = 0$. Because the intensity difference between the resonance-enhanced harmonics and the nonresonant harmonics is large, the intensity of the resonance-enhanced harmonics and the nonresonant harmonics cannot be displayed with the same color bar. In order to clearly show the variation of the harmonic intensity with the laser intensity, different color bars are used for the resonance-enhanced harmonics and the nonresonant harmonics, as shown in the lower and upper panels of Fig. 1(b), respectively. The color bars are marked with a linear color scale to reduce the modulation. The white arrows in the lower panel are used to mark the positions of the intensities of the resonance-enhanced harmonics (H21 and H23) which change significantly with the laser intensity. From the nonresonant harmonics shown in the upper panel we find that the harmonic cutoff increases gradually with an increase of the laser intensity, which is not of interest in the present work. We focus on the variation of the resonance-enhanced harmonic intensity with the laser intensity.

From the lower panel of Fig. 1(b) we find that the two resonance-enhanced harmonic orders do not change with an increase of the laser intensity, which can be illustrated through the Stark effect. The Stark effect will lead to an energy-level shift when the laser field is strong. For weakly bound states, such as the Rydberg state, continuous state, and higher excited state, the Stark effect leads to upshifting of the energy levels by approximately the ponderomotive energy U_p [40–42]. The low-order bound states close to the nucleus will obtain a little pondermotive energy due to the tight binding of the nucleus, which results in a smaller energy-level shift. The relevant bound states of the resonance-enhanced harmonics (H21 and H23) are the first excited state and the second excited state in our paper, which belong to the low-order bound state. Thus, the resonance-enhanced harmonics vary slowly with an increase of the laser intensity due to the small energy-level shift.

From the lower panel of Fig. 1(b) we also find that the harmonic intensities decrease gradually with an increase of the laser intensity. The intensity of H21 drops sharply around 6.0×10^{14} W/cm^2, which indicates that the energy level of the first excited state shifts significantly, and H21 gradually falls out of resonance around 6.0×10^{14} W/cm^2. The

intensity of H23 drops sharply around 2.0×10^{14} W/cm^2, which indicates that the energy level of the second excited state shifts significantly, and H23 gradually falls out of resonance around 2.0×10^{14} W/cm^2. In addition, H23 falls out of resonance before H21 with an increase of the laser intensity, which indicates that the energy-level shift of the second excited state is more significant than that of the first excited state.

To further illustrate the Stark effect on the resonance-enhanced harmonics for the different laser intensities we demonstrate the detailed Stark shift of the first excited state as a function of the laser intensity. In the external field, the analytical expression for the Stark shift can be obtained from the general formula derived in the second order of quantum-mechanical perturbation theory as [43,44]

$$\delta E_i = -\frac{1}{4}\left[\alpha_S^{nl} + \alpha_t^{nl}\frac{3m^2 - j(j+1)}{j(2j-1)}\right]E_0^2, \qquad (9)$$

where $\alpha_S^{nl} = \frac{n^4}{4Z^2}[4n^2 + 7l(l+1) + 14]$ and $\alpha_t^{nl} = -\frac{n^4}{4Z^4}[3n^2 + 11l(l+1) - 9]\frac{l}{2l+3}$ are the scalar and tensor polarizabilities, respectively; n, l, and m are the principal quantum number, orbital quantum number, and magnetic quantum number of the states, respectively; j is angular momentum of the states; and Z is the charge of the nucleus.

As is well known, perturbation theory is no longer applicable when the strong laser field interacts with atoms. From Table 1 of Ref. [44] we can see that the exact value of the Stark shift differs significantly from the value obtained from the perturbation theory when the laser intensity exceeds $E_0 = 0.2$ a.u. for the ground state of the hydrogen atom. If the laser intensity is increased further, the Stark shift of atomic levels loses all physical meaning [44]. Thus, the expression of the Stark shift is more applicable for the low laser intensity.

In order to ensure the applicability of the Stark shift expression, we take the Stark energy-level shift of the first excited state with a relatively low laser intensity (from 1.0×10^{14} to 6.0×10^{14} W/cm^2) as an example, as shown in Fig. 1(c). Here $n = 2$, $l = 1$, and $Z = 2$ correspond to the $2p$ energy level (the first excited state) of He$^+$ (we ignore the Stark shift of the ground state because the shift is too small). Figure 1(c) shows that the energy level of the first excited state shifts slightly below 0.045 a.u., which remains within the resonance-enhanced range of H21 (here the range between H20.5 and H21.5 is considered to be H21 resonance). With a further increase of the laser intensity, the Stark shift becomes larger, resulting in the weakening of the resonance-enhanced harmonic intensity, which agrees with the intensity of H21 dropping rapidly for 6.0×10^{14} W/cm^2, and the resonance-enhanced harmonic order does not change with an increase of the laser intensity, as shown in the lower panel of Fig. 1(b). Moreover, the Stark shift of the second excited state is larger than that of the first excited state due to the large principal quantum number n according to Eq. (9), resulting in the fact that H23 falls out of resonance before H21 with an increase of the laser intensity, which also agrees with that shown in the lower panel of Fig. 1(b).

Figure 2(a) shows that the intensities of the resonant (H21 and H23) and nonresonant (H31 and H37) harmonics vary
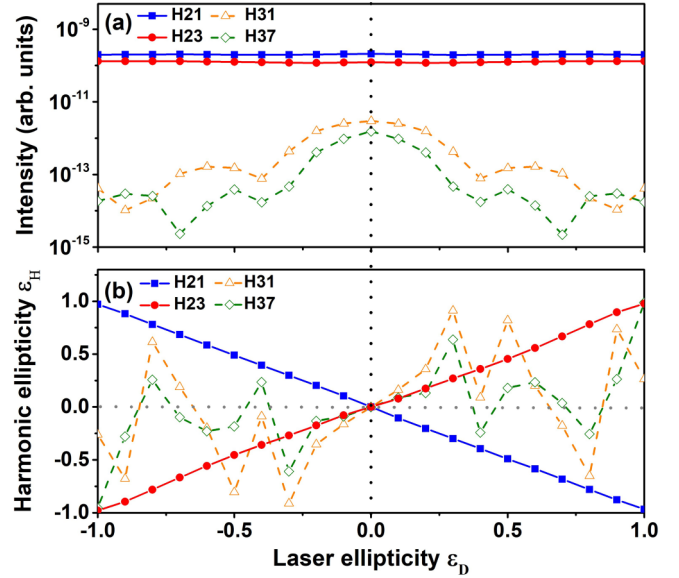

FIG. 2. (a) Intensity and (b) ellipticity of the resonant (H21 and H23) and nonresonant (H31 and H37) harmonics for different driving laser ellipticities. The black dotted and gray dotted lines indicate $\varepsilon_D = 0$ and $\varepsilon_H = 0$, respectively.

with the driving laser ellipticity ε_D. We find that the intensities of the resonant (H21 and H23) and nonresonant (H31 and H37) harmonics are symmetrical about $\varepsilon_D = 0$. The intensities of the resonance-enhanced (H21 and H23) harmonics remain unchanged with an increase of the absolute value of the driving laser ellipticity ε_D. For comparison with the resonance-enhanced harmonics, the nonresonant (H31 and H37) harmonic intensities varying with the driving laser ellipticity ε_D are also shown in Fig. 2(a), where the ionization threshold order is 31 and the order above threshold is 37. It is observed that the intensities of the nonresonant (H31 and H37) harmonics decrease with an increase of the absolute value of driving laser ellipticity ε_D, which is in agreement with that illustrated in Fig. 1(a).

Surprisingly, H21 and H23 harmonics are also generated in the circularly polarized laser field, which is contrary to the expected result that the harmonics cannot be generated when the circularly polarized laser field interacts with an isotropic medium according to the conservation of angular momentum [45]. However, the resonance enhancements of H21 and H23 are only due to the radiative transitions between the ground state and excited states, which is independent of the polarization of the laser field. Moreover, the intrinsic nonlinear phenomena, such as radiative phenomena, are not considered in Ref. [45]. Thus, the resonance enhancements of H21 and H23 driven by the circularly polarized laser field can be generated.

In addition, we also demonstrated the transition rates from the ground state to the first excited state ($|0\rangle \rightarrow |1\rangle$) and the ground state to the second excited state ($|0\rangle \rightarrow |2\rangle$) with different driving laser ellipticity (the results are not shown here). The result shows that the $|0\rangle \rightarrow |1\rangle$ and $|0\rangle \rightarrow |2\rangle$ transitions can occur for each driving laser ellipticity, which indicates that the resonance-enhanced harmonics (H21 and H23) can

be generated for each driving laser ellipticity, including the circularly polarized laser field. Moreover, the time of the high transition rates agrees with the time generated the resonance-enhanced harmonics with high intensity.

Figure 2(b) shows the resonance-enhanced (H21 and H23) and nonresonant (H31 and H37) harmonic ellipticities ε_H as a function of different driving laser ellipticities ε_D. The black and gray dotted lines indicate $\varepsilon_D = 0$ and $\varepsilon_H = 0$, respectively. We see that the ellipticities of the resonance-enhanced (H21 and H23) and nonresonant (H31 and H37) harmonics are centrosymmetric about the original point ($\varepsilon_D = 0$ and $\varepsilon_H = 0$). This indicates that the helicity of the harmonics is opposite and the magnitudes of the harmonic ellipticities are equal for the right laser helicity $\varepsilon_D > 0$ and the left laser helicity $\varepsilon_D < 0$. For the resonance-enhanced harmonics (H21 and H23) we observe that the absolute value of the harmonic ellipticity first decreases linearly from $|\varepsilon_H| = 1.0$ to $|\varepsilon_H| = 0$ with driving laser ellipticity varying from $\varepsilon_D = -1.0$ to $\varepsilon_D = 0$ and then increases from $|\varepsilon_H| = 0$ to $|\varepsilon_H| = 1.0$ with driving laser ellipticity varying from $\varepsilon_D = 0$ to $\varepsilon_D = 1.0$. In short, the absolute value of the harmonic ellipticity becomes larger as the absolute value of the driving laser ellipticity increases. This means that the ellipticity of the resonance-enhanced harmonics can be tuned from linear to circular with the driving laser ellipticity varying from $\varepsilon_D = 0$ to $\varepsilon_D = \pm 1.0$ and the harmonics with high ellipticity and high intensity can be achieved by adjusting the driving laser ellipticity. However, the ellipticities of the nonresonant harmonics (H31 and H37) oscillate greatly with the driving laser ellipticity from $\varepsilon_D = -1.0$ to $\varepsilon_D = 1.0$.

From the numerical relationship between the resonance-enhanced harmonic ellipticities ε_H and the driving laser ellipticities ε_D as shown in Fig. 2(b) we obtain the scaling rule of $\varepsilon_H \propto -|\varepsilon_D|^{0.98}$ ($\varepsilon_H \propto |\varepsilon_D|^{0.98}$) for the ellipticity of H21 and that of $\varepsilon_H \propto |\varepsilon_D|^{0.9}$ ($\varepsilon_H \propto -|\varepsilon_D|^{0.9}$) for H23 when $\varepsilon_D > 0$ ($\varepsilon_D < 0$), respectively, which means that the resonance-enhanced harmonic ellipticities are approximately equal to the driving laser ellipticities without considering the $\pm$ sign. In Ref. [46] Gruson *et al.* obtained that the ellipticity of the harmonics is about the same as that of the driving laser from Ar driven by the EP laser field which is formed by two orthogonal linearly polarized laser pulses. Our result is similar to that illustrated in Ref. [46]. Moreover, the ellipticity scaling rule of $\varepsilon_{EUV} \propto \varepsilon_{IR}^{\sigma}$ was also illustrated experimentally in Refs. [11,47], where ε_{EUV} and ε_{IR} are the ellipticities of the high harmonics and the driving laser field, respectively, and σ is the ellipticity scaling coefficient. In Ref. [11] Huang *et al.* obtained the ellipticity scaling rule of $\varepsilon_{EUV} \propto \varepsilon_{IR}^{4.5-4.8}$ from Ar driven by the two counterrotating few-cycle laser beams. In Ref. [47] Chang *et al.* obtained the ellipticity scaling rule of $\varepsilon_{EUV} \propto \varepsilon_{IR}^{2.2-5.8}$, $\varepsilon_{EUV} \propto \varepsilon_{IR}^{2.5-8.3}$, and $\varepsilon_{EUV} \propto \varepsilon_{IR}^{5.3-13.5}$ for Ar, Kr, and Xe, respectively, driven by the two noncollinear counterrotating laser fields. They found that the polarization state of a single harmonic can be controlled from linear to highly elliptical by adjusting the ellipticity of the driving laser pulses. The ellipticity scaling rule demonstrated in Fig. 2(b) is similar to that demonstrated in Refs. [11,47]. It is possible that our result can provide an accessible method to characterize the polarization properties of the laser by the resonance-enhanced harmonic ellipticity.
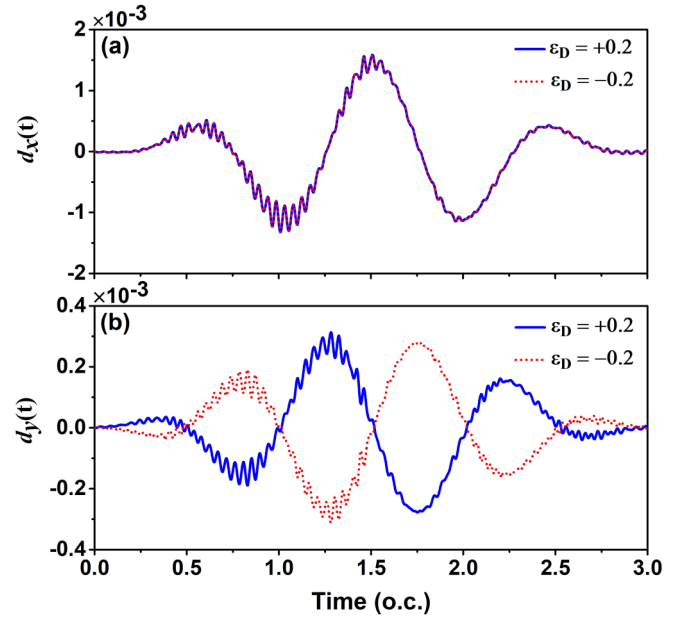

FIG. 3. The (a) x and (b) y components of the time-dependent dipole acceleration for different driving laser helicities. The blue solid line and the red dotted line represent the results of $\varepsilon_D = 0.2$ ($\varepsilon_D > 0$) and $\varepsilon_D = -0.2$ ($\varepsilon_D < 0$), respectively.

Figure 3 shows the x and y components of the dipole acceleration expressed in Eq. (3) for different driving laser helicities. Here we take the laser ellipticities $\varepsilon_D = \pm 0.2$ as an example. The blue solid line and the red dotted line represent the results of $\varepsilon_D = +0.2$ ($\varepsilon_D > 0$) and $\varepsilon_D = -0.2$ ($\varepsilon_D < 0$), respectively. From Fig. 3(a) we find that the x component of the dipole acceleration is identical for different driving laser helicities [$\varepsilon_D = +0.2$ ($\varepsilon_D > 0$) and $\varepsilon_D = -0.2$ ($\varepsilon_D < 0$)]. Thus, $d_x^R(t) = d_x^L(t)$ can be obtained when the driving laser helicity changes. Here the superscripts R and L represent the right laser helicity ($\varepsilon_D > 0$) and the left laser helicity ($\varepsilon_D < 0$), respectively. From Fig. 3(b) we see that the y component of the dipole acceleration is equal in magnitude but opposite in sign for the right laser helicity [$\varepsilon_D = +0.2$ ($\varepsilon_D > 0$)] and the left laser helicity [$\varepsilon_D = -0.2$ ($\varepsilon_D < 0$)]; thus $d_y^R(t) = -d_y^L(t)$ can be obtained when the driving laser helicity changes.

The x and y components of the dipole acceleration in the frequency domain expressed in Eq. (7) for the right laser helicity ($\varepsilon_D > 0$) and the left laser helicity ($\varepsilon_D < 0$) can be expressed as $a_x^R(\omega) = a_x^L(\omega)$ and $a_y^R(\omega) = -a_y^L(\omega)$ due to $d_x^R(t) = d_x^L(t)$ and $d_y^R(t) = -d_y^L(t)$. Thus Eq. (6) can be written as $a_{\pm}^R = \frac{1}{\sqrt{2}}[a_x^R(\omega) \pm ia_y^R(\omega)] = \frac{1}{\sqrt{2}}[a_x^L(\omega) \mp ia_y^L(\omega)] = a_{\mp}^L$ (i.e., $a_+^R = a_-^L$, $a_-^R = a_+^L$). The ellipticity of the harmonics of Eq. (5) can be expressed as $\varepsilon_H^R = \frac{(|a_+^R| - |a_-^R|)}{(|a_+^R| + |a_-^R|)} = \frac{(|a_-^L| - |a_+^L|)}{(|a_-^L| + |a_+^L|)} = -\varepsilon_H^L$, which means that the helicity of the harmonics is opposite and the magnitude of the harmonic ellipticity is equal for the right laser helicity ($\varepsilon_D > 0$) and the left laser helicity ($\varepsilon_D < 0$). This analysis is in agreement with that illustrated in Fig. 2(b).

In order to obtain high ellipticity, the amplitudes of the x and y components of the harmonics should be comparable and
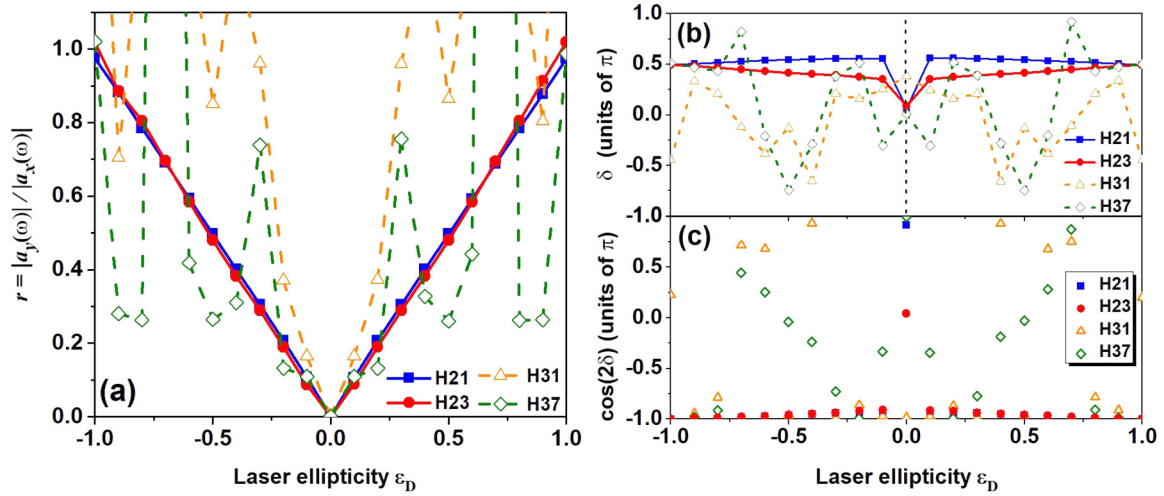
FIG. 4. (a) Ratio $r = |a_y(\omega)|/|a_x(\omega)|$ of the x and y components of the dipole acceleration in the frequency domain for different driving laser ellipticities. (b) Phase difference δ of the x and y components of the harmonics and (c) cosine value of 2δ corresponding to (b) for the resonant (H21 and H23) and nonresonant (H31 and H37) harmonics for different driving laser ellipticities.

their phase difference should be close to $\frac{\pi}{2}$ [36]. Figure 4(a) shows the ratio $r = |a_y(\omega)|/|a_x(\omega)|$ of the x and y components of the dipole acceleration in the frequency domain of the resonant (H21 and H23) and nonresonant (H31 and H37) harmonics for different driving laser ellipticities ε_D. We find that the ratio r is irregular with large oscillations for the nonresonant (H31 and H37) harmonics, while the expression $r \approx |\varepsilon_D|$ can be obtained for the resonance-enhanced (H21 and H23) harmonics. Due to the expressions of $r \approx |\varepsilon_D|$ and Eq. (8), the ellipticity of the resonance-enhanced harmonics can be expressed as

$$\varepsilon_H \approx \pm \sqrt{\frac{1 + \varepsilon_D^2 - \sqrt{1 + \varepsilon_D^4 + 2\varepsilon_D^2 \cos(2\delta)}}{1 + \varepsilon_D^2 + \sqrt{1 + \varepsilon_D^4 + 2\varepsilon_D^2 \cos(2\delta)}}}. \quad (10)$$

Figure 4(b) shows the phase differences δ of the x and y components of the harmonics. We find that the phase differences δ of the x and y components of the resonance-enhanced harmonics (H21 and H23) are closer to $\frac{\pi}{2}$ with an increase of the absolute value of the driving laser ellipticity, which is in agreement with the harmonic ellipticity becoming larger as the absolute value of the driving laser ellipticity increases, as shown in Fig. 2(b). The phase differences of the nonresonant harmonics are disorganized, which corresponds to the irregular ellipticity as shown in Fig. 2(b). In addition, the values of $\cos(2\delta)$ for the resonant and nonresonant harmonics for different driving laser ellipticities are shown in Fig. 4(c). We see that the value of $\cos(2\delta)$ for the resonance-enhanced harmonics is approximately -1, i.e., $\cos(2\delta) \approx -1$, while that of the nonresonant harmonics is irregular. Thus, Eq. (10) for the ellipticity of the resonance-enhanced harmonics can be further expressed as

$$\varepsilon_H \approx \pm \sqrt{\frac{1 + \varepsilon_D^2 - \sqrt{1 + \varepsilon_D^4 - 2\varepsilon_D^2}}{1 + \varepsilon_D^2 + \sqrt{1 + \varepsilon_D^4 - 2\varepsilon_D^2}}} = \pm\varepsilon_D. \quad (11)$$

This means that the resonance-enhanced harmonic ellipticity ε_H is approximately equal to the driven laser ellipticity ε_D regardless of the $\pm$ sign, which is in agreement with that illustrated in Fig. 2(b).

To understand the significant enhancement of the resonance-enhanced harmonics, we investigate the time dependence of the emission efficiency of the selected harmonics via the time-frequency analysis [48]. Figure 5 shows the time profile of the resonant (H21 and H23) and nonresonant (H31 and H37) harmonics with the driving laser ellipticities from $\varepsilon_D = 0$ to 0.6, respectively. From Figs. 5(a)–5(d) we find that the amplitude of the time profiles of the resonance-enhanced harmonics is stronger than that of the nonresonant harmonics, which is in agreement with that illustrated in Fig. 2(a). As the driving laser ellipticity increases, the amplitudes of the resonance-enhanced harmonics are almost unchanged, while those of the nonresonant harmonics decrease, which is also in agreement with that illustrated in Fig. 2(a).

For the resonance-enhanced harmonics (H21 and H23) as shown by the blue solid and red dashed lines in Figs. 5(a)–5(d) we find that the time profiles of H21 and H23 harmonics are continuous over time, which means that the ionized electrons immediately return and continuously recollide with the parent ion; this process is dominated by the multiphoton mechanism [17,39]. Thus, the continuous collisions of the electron with the parent ion due to multiphoton resonance result in the enhancement of the resonant harmonics (H21 and H23). For the nonresonant harmonics (H31 and H37) as shown by the orange dash-dotted and green dotted lines in Figs. 5(a)–5(d) we find that the time profiles of H31 and H37 are mainly distributed from $t = 0$ to 2.0 o.c. and are weak from $t = 2.0$ to 3.0 o.c.. In particular, for $\varepsilon_D = 0.6$, the time profiles of the nonresonant harmonics are almost 0 from $t = 1.5$ to 3.0 o.c. The time profiles of H31 and H37 twice per cycle drop to approximately 0, as shown by the yellow and green arrows in Figs. 5(a)–5(d), where the yellow and the green arrows indicate the times that the time profiles of H31 and H37 drop near 0, respectively. The result means that the ionized electrons recollide with the parent ion twice per
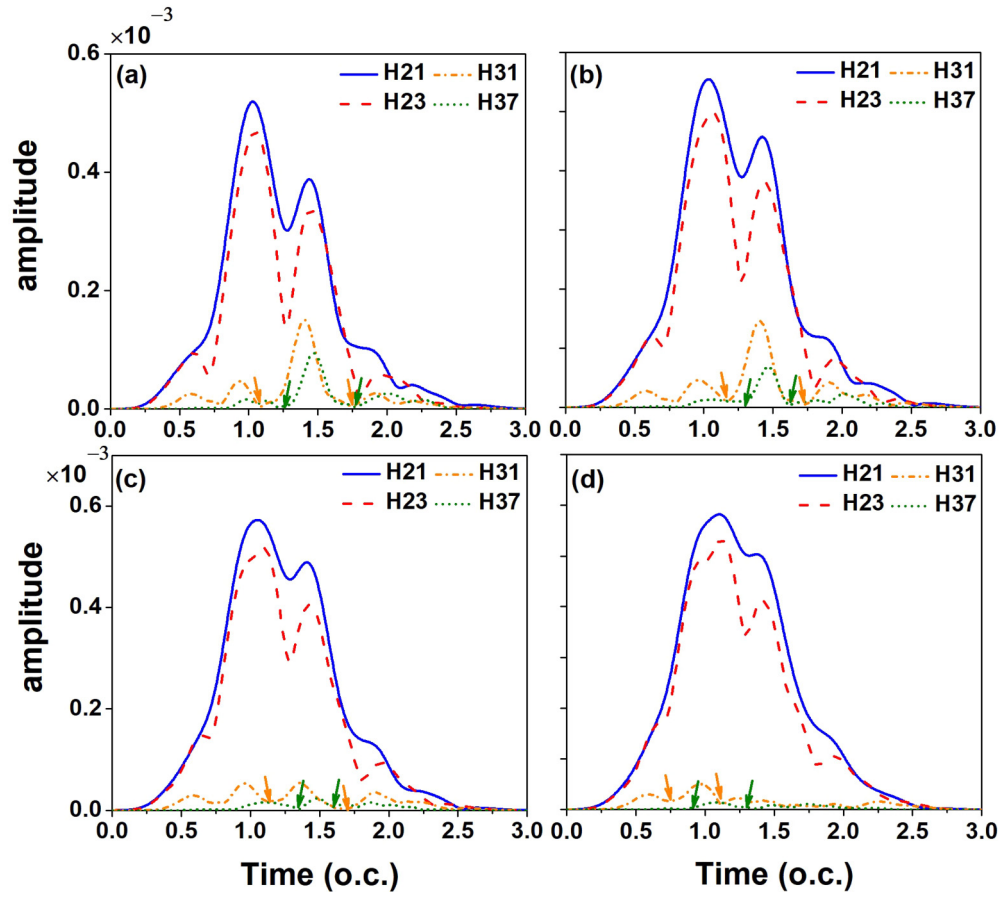
FIG. 5. Time profile of the amplitude of the harmonics via the time-frequency analysis for the resonant (H21 and H23) and nonresonant (H31 and H37) harmonics with the driving laser ellipticity (a) $\varepsilon_D = 0$, (b) $\varepsilon_D = 0.2$, (c) $\varepsilon_D = 0.4$, and (d) $\varepsilon_D = 0.6$. The blue solid, red dashed, orange dash-dotted, and green dotted lines indicate H21, H23, H31, and H37, respectively. The yellow and the green arrows indicate the times that the time profiles of H31 and of H37 drop close to 0, respectively.

cycle and this process is dominated by the three-step model [17,39].

In short, our results indicate that the enhancement of the harmonics can be attributed to the multiphoton resonance and the multiphoton mechanism does not contribute to the HHG with the increase of the harmonic orders, resulting in the weak nonresonant harmonic intensity. In Ref. [39] Chu and Groenenboom investigated the resonance-enhanced HHG from N_2 driven by a linearly polarized laser. The result indicated that the harmonic maxima are caused by resonance-enhanced multiphoton excitation and the contribution of multiphoton resonance decreases with the increase of the harmonic orders. Our result is agreement with that demonstrated in Ref. [39].

In addition, the frequency of electrons returning to the parent ion decreases for the nonresonant harmonics compared to that of the resonance-enhanced harmonics in the same time, which leads to lower intensities of the nonresonant harmonics than those of the resonance-enhanced harmonics. Thus, we can conclude that the multiple collisions of the electron with the parent ion due to multiphoton resonance are the origin of the resonance enhancement of the harmonics. In Ref. [49] Ganeev *et al.* demonstrated that the resonance enhancement of a single high-order harmonic from an ion driven by a femtosecond pulse is attributed to multiple collisions of electron

trajectories with the origin due to multiphoton resonance. Our result is consistent with that illustrated in Ref. [49].

IV. CONCLUSION

To summarize, we have investigated the resonance-enhanced HHG for He^+ driven by an EP laser field. We showed that the intensities of the resonance-enhanced harmonics remain unchanged and are approximately two orders of magnitude higher than those of nonresonant harmonics, while the intensities of the nonresonant harmonics decrease rapidly with the driving laser ellipticity. The first resonance-enhanced harmonic is generated due to the transition between the ground state and the first excited state; the second one is generated due to the transition between the ground state and the second excited state. Our results also demonstrated that the resonance enhancements of the harmonics originate from the continuous return of electrons to the parent ion. The two resonance-enhanced harmonic intensities decrease gradually and orders do not change with the increase of the laser intensity, which can be illustrated through the Stark effect. Moreover, we found that the ellipticity of the resonance-enhanced harmonics is more regular than that of the nonresonant harmonics. The resonance-enhanced harmonic ellipticity and the driving laser ellipticity are

approximately the same regardless of the $\pm$ sign. This means that our results provide an accessible method to characterize the polarization properties of the laser by the resonance-enhanced harmonic ellipticity. Our results offer a way to generate quasimonochromatic CP EUV radiation with high intensity.

[1] P. B. Corkum, Phys. Rev. Lett. **71**, 1994 (1993).

[2] X. Cao, S. Jiang, C. Yu, Y. Wang, L. Bai, and R. Lu, Opt. Express **22**, 26153 (2014).

[3] M.-C. Chen, P. Arpin, T. Popmintchev, M. Gerrity, B. Zhang, M. Seaberg, D. Popmintchev, M. M. Murnane, and H. C. Kapteyn, Phys. Rev. Lett. **105**, 173901 (2010).

[4] P.-C. Li, X.-X. Zhou, G.-L. Wang, and Z.-X. Zhao, Phys. Rev. A **80**, 053825 (2009).

[5] N. Böwering, T. Lischke, B. Schmidtke, N. Müller, T. Khalil, and U. Heinzmann, Phys. Rev. Lett. **86**, 1187 (2001).

[6] R. Cireasa, A. E. Boguslavskiy, B. Pons, M. C. H. Wong, D. Descamps, S. Petit, H. Ruf, N. Thiré, A. Ferré, J. Suarez, J. Higuet, B. E. Schmidt, A. F. Alharbi, F. Légaré, V. Blanchet, B. Fabre, S. Patchkovskii, O. Smirnova, Y. Mairesse, and V. R. Bhardwaj, Nat. Phys. **11**, 654 (2015).

[7] T. Fan, P. Grychtol, R. Knut, C. Hernández-García, D. D. Hickstein, D. Zusin, C. Gentry, F. J. Dollar, C. A. Mancuso, C. W. Hogle, O. Kfir, D. Legut, K. Carva, J. L. Ellis, K. M. Dorney, C. Chen, O. G. Shpyrko, E. E. Fullerton, O. Cohen, P. M. Oppeneer *et al.*, Proc. Natl. Acad. Sci. USA **112**, 14206 (2015).

[8] J. L. Ellis, K. M. Dorney, D. D. Hickstein, N. J. Brooks, C. Gentry, C. Hernández-García, D. Zusin, J. M. Shaw, Q. L. Nguyen, C. A. Mancuso, G. S. M. Jansen, S. Witte, H. C. Kapteyn, and M. M. Murnane, Optica **5**, 479 (2018).

[9] L. Barreau, K. Veyrinas, V. Gruson, S. J. Weber, T. Auguste, J. F. Hergott, F. Lepetit, B. Carré, J. C. Houver, D. Dowek, and P. Saliéres, Nat. Commun. **9**, 4727 (2018).

[10] K. J. Yuan and A. D. Bandrauk, Phys. Rev. A **97**, 023408 (2018).

[11] P. C. Huang, C. Hernández-García, J. T. Huang, P. Y. Huang, C. H. Lu, L. Rego, D. D. Hickstein, J. L. Ellis, A. Jaron-Becker, A. Becker, S. D. Yang, C. G. Durfee, L. Plaja, H. C. Kapteyn, M. M. Murnane, A. H. Kung, and M. C. Chen, Nat. Photon. **12**, 349 (2018).

[12] C. Zhai, R. Shao, P. Lan, B. Wang, Y. Zhang, H. Yuan, S. M. Njoroge, L. He, and P. Lu, Phys. Rev. A **101**, 053407 (2020).

[13] X.-X. Huo, Y.-H. Xing, T. Qi, Y. Sun, B. Li, J. Zhang, and X.-S. Liu, Phys. Rev. A **103**, 053116 (2021).

[14] D. Habibović and D. B. Milošević, Photonics **7**, 110 (2020).

[15] S. Odžak and D. B. Milošević, Phys. Rev. A **82**, 023412 (2010).

[16] V. V. Strelkov, M. A. Khokhlova, A. A. Gonoskov, I. A. Gonoskov, and M. Y. Ryabikin, Phys. Rev. A **86**, 013404 (2012).

[17] H. Yang, P. Liu, R. Li, and Z. Xu, Opt. Express **21**, 28676 (2013).

[18] Y. Li, X. Zhu, Q. Zhang, M. Qin, and P. Lu, Opt. Express **21**, 4896 (2013).

[19] E. Fiordilino, F. Morales, G. Castiglia, P. P. Corso, R. Daniele, and V. V. Strelkov, J. Opt. Soc. Am. B **34**, 18 (2017).

[20] F. J. Sun, C. Chen, W. Y. Li, X. Liu, W. Li, and Y. J. Chen, Phys. Rev. A **103**, 053108 (2021).

[21] P. Antoine, B. Carré, A. L'Huillier, and M. Lewenstein., Phys. Rev. A **55**, 1314 (1997).

[22] J. Heslar, D. A. Telnov, and S.-I. Chu, Phys. Rev. A **93**, 063401 (2016).

[23] Y. Zeng, H. Qian, M. J. Rozin, Z. Liu, and A. R. Tao, Adv. Funct. Mater. **28**, 1803019 (2018).

[24] S. Kazamias, D. Douillet, F. Weihe, C. Valentin, A. Rousse, S. Sebban, G. Grillon, F. Augé, D. Hulin, and P. Balcou, Phys. Rev. Lett. **90**, 193901 (2003).

[25] M. Suzuki, M. Baba, R. Ganeev, H. Kuroda, and T. Ozaki, Opt. Lett. **31**, 3306 (2006).

[26] S. Camp, K. J. Schafer, and M. B. Gaarde, Phys. Rev. A **92**, 013404 (2015).

[27] K. Ishikawa, Phys. Rev. Lett. **91**, 043002 (2003).

[28] K. N. Avanaki, D. A. Telnov, H. Z. Jooya, and S.-I. Chu, Phys. Rev. A **92**, 063811 (2015).

[29] V. Strelkov, Phys. Rev. Lett. **104**, 123901 (2010).

[30] R. Taïeb, V. Véniard, J. Wassaf, and A. Maquet, Phys. Rev. A **68**, 033403 (2003).

[31] A. Ferré, C. Handschin, M. Dumergue, F. Burgy, A. Comby, D. Descamps, B. Fabre, G. A. Garcia, R. Géneaux, L. Merceron, E. Mével, L. Nahon, S. Petit, B. Pons, D. Staedter, S. Weber, T. Ruchon, V. Blanchet, and Mairesse, Nat. Photon. **9**, 93 (2015).

[32] M. A. Khokhlova, M. Y. Emelin, M. Y. Ryabikin, and V. V. Strelkov, Phys. Rev. A **103**, 043114 (2021).

[33] Y. H. Lai, K. S. Rao, J. Liang, X. Wang, C. Guo, W. Yu, and W. Li, Opt. Lett. **46**, 2372 (2021).

[34] Q. Su and J. H. Eberly, Phys. Rev. A **44**, 5997 (1991).

[35] X. Zhang, X. Zhu, X. Liu, D. Wang, Q. Zhang, P. Lan, and P. Lu, Opt. Lett. **42**, 1027 (2017).

[36] B. Zhang and Z. X. Zhao, Chin. Phys. Lett. **30**, 023202 (2013).

[37] P.-C. Li, Z.-B. Wang, and S.-I. Chu, Phys. Rev. A **103**, 043113 (2021).

[38] X. B. Bian and A. D. Bandrauk, Appl. Sci. **3**, 267 (2013).

[39] X. Chu and G. C. Groenenboom, Phys. Rev. A **87**, 013434 (2013).

[40] R. R. Freeman, P. H. Bucksbaum, H. Milchberg, S. Darack, D. Schumacher, and M. E. Geusic, Phys. Rev. Lett. **59**, 1092 (1987).

[41] C. F. de Morisson Faria, R. Kopold, W. Becker, and J. M. Rost, Phys. Rev. A **65**, 023404 (2002).

[42] M. Protopapas, C. H. Keitel, and P. L. Knight, Rep. Prog. Phys. **60**, 389 (1997).

[43] A. A. Krylovetsky, N. L. Manakov, and S. I. Marmo, Laser Phys. **7**, 781 (1997).

[44] N. B. Delone and V. P. Krainov, Phys. Usp. **42**, 669 (1999).

[45] N. Bloembergen, J. Opt. Soc. Am. **70**, 1429 (1980).

[46] V. Gruson, S. J. Weber, L. Barreau, J. F. Hergott, F. Lepetit, T. Auguste, B. Carré, P. Salières, and T. Ruchon, J. Opt. Soc. Am. B **35**, A15 (2018).

[47] K. Y. Chang, L. C. Huang, K. Asaga, M. S. Tsai, L. Rego, P. C. Huang, H. Mashiko, K. Oguri, C. Hernández-García, and M. C. Chen, Optica **8**, 484 (2021).

[48] P. Antoine, B. Piraux, and A. Maquet, Phys. Rev. A **51**, R1750(R) (1995).

[49] R. A. Ganeev, M. Suzuki, M. Baba, H. Kuroda, and T. Ozaki, Opt. Lett. **31**, 1699 (2006).